Highly porous and flexible capacitive humidity sensor based on self-assembled graphene oxide sheets on a paper substrate

R. Alrammouz, Jean Podlecki, A. Vena, Ricardo Garcia, P. Abboud, R. Habchi, B. Sorli

Highly porous and flexible capacitive humidity sensor based on self-assembled graphene oxide sheets on a paper substrate

R.Alrammouz[a,b], J. Podlecki[a], A. Vena[a], R. Garcia[a], P. Abboud[b], R. Habchi[b], B. Sorli[a]

a. Institut d'Electronique et des Systèmes (IES, UMR5214), Université de Montpellier (UM), Montpellier, France ;
b. EC2M, Faculty of Sciences, Campus Pierre Gemayel, Lebanese University (UL), Fanar, 90656, Lebanon ;

*Corresponding Author: Rouba Alrammouz
E-mail : roubarammouz@gmail.com

Abstract

This paper reports the fabrication of capacitive humidity sensors by integrating a graphene oxide sensing layer inside paper substrates. Graphene oxide sheets were self-assembled on the papers' fibers. A comparative study between several sensors with different concentrations of graphene oxide and different processing times in the graphene oxide suspension is reported. Its aim is to optimize the sensing layer in terms of concentration and thickness towards the fabrication of highly sensitive and porous sensors. The morphology of the fabricated sensors was characterized using scanning electron microscopy, their structure and chemical composition using Raman and infrared spectroscopies. The washability and mechanical strength of the graphene oxide coated paper were tested in water and in an ultrasonic bath. Last, the sensing capabilities of the fabricated devices were tested for a relative humidity ranging from 30% to 90% RH. The optimal sensor is highly porous, hydrophobic and exhibits a good response towards humidity with a low hysteresis. This work presents a low cost alternative for the use of polymers and coated-papers as substrates for flexible electronics. It is also a first step towards the integration of flexible electronics into substrates, which enables the fabrication of highly porous, economical and flexible devices ideal for air flow monitoring, e-dressings and e-textiles.

Keywords: Capacitive sensor; humidity; graphene oxide; porous paper; flexible

1. Introduction

Controlling and monitoring humidity is of increasing interest in many fields such as meteorology, agriculture (greenhouse air control), HVAC (Heating, Ventilation and Air-Conditioning), automobile (development of defoggers), medicine and pharmaceuticals (respiratory equipment), medicine processing, and food logistics [1]. The growing need for humidity sensors requires the development of low cost, bendable, wearable and portable devices for their potential application in smart-packaging and e-textiles. Flexible humidity sensors use two main sensing principles: capacitive and resistive. The resistive transducing principle is based on changes in the resistance of the sensing layer whereas the capacitive transducing principle is based on a change in its capacitance. The main advantage of capacitive sensors over resistive ones is their lower power consumption and the possibility of their implementation in high frequency applications. Several materials have been investigated for their humidity sensing capabilities, such as polymers [2-11], biopolymers such as wheat gluten [12-15], metal oxides [16-18], carbon nanotubes [19], transition metal dichalcogenides (TDMCs) [20, 21] and cellulose [22, 23].

Recently, graphene attracted the attention of researchers for the development of flexible gas sensors due to its high carrier mobility, its large specific surface ($2600 m^2.g^{-1}$), its pliability and its excellent mechanical strength. The main drawback of graphene is that its deposition requires high temperatures (chemical vapor deposition). As a result, graphene is usually deposited on a rigid substrate prior to its transfer to a flexible substrate [24, 25]. Graphene oxide is a derivative of graphene that offers the possibility of room temperature deposition using techniques as simple as coating and self-assembly. Graphene oxide has been widely investigated for its gas sensing capabilities, of which humidity sensing [26]. In fact, graphene oxide consists of graphene sheets functionalized with carbonyl (-COOH), hydroxyl (-OH) and epoxy (=O). The GO's hydrophilic functional groups (hydroxyl and epoxy) enhance the adsorption and desorption of water molecules and thus enhance the sensitivity of the material. The literature reports several capacitive [23, 27-31] and resistive [32-39] graphene oxide flexible gas sensors. Several

graphene oxide based capacitive humidity sensors were also reported. For example, three graphene oxide capacitive humidity sensors functionalized with ZnO, SnO_2 and PDDA on polyimide substrates using the layer by layer self-assembly technique were reported by Zhang et al. [27-29]. Ali et al. fabricated a capacitive humidity sensor based on a graphene oxide / methylred sensing layer deposited on a PET substrate [31]. Another flexible humidity sensor on a PET substrate is proposed by Kafy et al. [23]. The sensor uses a drop-casted cellulose nanocrystals and graphene oxide composites layer as a sensing element. However, all the reported sensors rely on the deposition of the sensing layer on the surface of a polymeric substrate. An interesting approach is to integrate a sensing layer inside the substrate. This can only be achieved using cellulosic bare paper substrates. This type of substrate is not only low cost, but also offers a large specific area. This increases the sensitivity of the device by increasing the number of gas adsorption sites on its surface. Moreover, cellulose is recyclable, renewable and biodegradable. Cellulose based materials can also be incinerated which can facilitate the disposal of electronic waste. In addition, integrating electronic devices inside paper substrates enables several applications such as e-textiles, e-dressings and low-cost disposable applications. The literature reports the fabrication of CNT based resistive gas sensors inside cellulosic paper using drop-casting, inkjet-printing, plasma jet printing and papermaking filtration as deposition techniques [19, 40-42]. The sensors were able to detect humidity, chlorine, ammonia and nitrogen dioxide.

This paper reports the fabrication of a capacitive humidity sensor based on self-assembled graphene oxide on the fibers of a paper. Sensors with different concentrations of graphene oxide and different immersion times in a GO suspension were fabricated. The morphology of the sensors was characterized using scanning electron microscopy (SEM). The chemical structure of the sensors was characterized using Raman and FTIR spectroscopies. The washability and the mechanical strength of the sensors were also characterized using SEM and Raman spectroscopy after washing them in water and in an ultrasonic bath. The graphene oxide conductivity was measured using a four probe testing bench. A comparative study between the fabricated sensors was conducted. Its aim was to optimize the sensing layer in terms of concentration and immersion time in the GO-suspension. This study was based on the relative change in the capacitance of the GO-coated papers under 90% RH for a frequency range of 500 Hz to 200 kHz. The optimal sensor's sensing capabilities were also tested in terms of repeatability, reversibility, flexibility, temperature dependence and reproducibility. This work presents a novel approach towards the fabrication of highly porous, water resistant, disposable, flexible gas sensors that enable new unconventional applications such as air flow monitoring and e-dressings.

2. Materials and methods

2.1. Device fabrication

The sensors were fabricated by self-assembly of graphene oxide around the paper's fibers (figure 1.a). A 4 mg/mL solution of graphene oxide was purchased from Graphenea and used without any further treatment. Three graphene oxide suspensions were prepared by diluting the purchased solution in deionized water with a dilution ratio of 1:1, 1:2 and 1:4. Paper substrates (purchased from Schweitzer Mauduit SWM) were cleaned using ethanol, dried at room temperature and cut into 2 cm x 2 cm pieces.

The prepared substrates were immersed in the 1 mg/mL, 2 mg/mL and 4 mg/mL graphene oxide suspensions for 10, 20, 30, 40 and 60 minutes each. The sensors were afterwards dried at room temperature. Last, aluminum interdigitated electrodes (IDEs) were deposited using thermal evaporation under vacuum. The electrodes were 500 nm thick and the space between electrodes was 500 µm (figure 1.b.). This IDEs geometry provides an effective sensing area of 1.015 cm^2. We should note that in the following sections the immersion time of the paper in the graphene oxide suspension will be referred to as treatment time.

2.2. Characterization

The morphology of the sensing layer was observed using a Hitachi S4800 scanning electron microscope at an acceleration voltage of 20 kV. The chemical structure of the fabricated sensors was analyzed using Raman and

Fourier-transform infrared spectroscopies. The Raman spectrum of the graphene oxide was observed using a Horiba Xplora Raman microscope with an excitation wavelength of 532 nm. Fourier infrared spectra was collected using an IFS66V FTIR spectrometer in Attenuated Total Reflectance (ATR) mode. Current-voltage curves were measured using a Cascade Microtech M150 four-probe tester and an Agilent technologies B1500A semi-conductor device analyzer under ambient conditions.

2.3. Measurement setup

Humidity measurements were carried out in an Espec SH-242 climatic chamber with a humidity range of 30%-90% at 22˚C. The sensors were connected to a 4192A LF impedance analyzer (5 Hz-13 MHz, Helwett-Packard) using a two probe testing device fabricated by our team (Figure 2.). Since graphene oxide best operate at relatively low frequencies [23, 27, 30], the sensors' response to humidity was characterized for a frequency range of [0.5 , 200] kHz. The sensors' response towards humidity was measured for a range of [30,90]% RH. All humidity tests were performed at room temperature (22˚C). The relative response towards humidity is defined as the relative change in the capacitance of the sensing layer (1):

$$S_R(\%) = \Delta C/C_0 \times 100 = (C_g - C_0)/C_0 \times 100 \quad (1)$$

where C_g is the capacitance under humidity, and C_0 the base capacitance under 30% RH. The sensitivity of the sensor is given by:

$$S_{(pF/\%RH)} = \Delta C/\Delta RH \quad (2)$$

The response time is the time taken by the sensor to reach 90% of its final state, and the recovery time is the time taken by the sensor to go back to its initial state after turning the target gas off.

3. Results and discussion

3.1. Morphology

Humidity sensors were fabricated by self-assembly of graphene oxide sheets inside the paper with different concentrations and treatment times. The morphology of the deposited layer shows several ripples and wrinkles, implicating thus the wrapping of graphene oxide sheets around the fibers. Moreover, SEM images show that the sensing layer's thickness increases with the increasing concentration of the graphene oxide suspension (figure 3.b,c,d) and with the increasing processing time in the graphene oxide suspension (figure 4.).

Thickness measurements were carried out on 4 mg/mL graphene oxide coated papers using SEM. Figure 5 shows the images of a transversal cut of three 4 mg/mL GO-coated papers with different processing times: 10, 30 and 60 min. The *thickness* of the 4 mg/mL graphene oxide sensing layer exponentially increases with the treatment time *t* in minutes (figure 6.a.):

$$thickness_{4\ mg/mL} = 0.1974.e^{0.03159.t}\ (\mu m) \quad (3)$$

Moreover, standard error calculations, plotted in figure 6.a., show that the uniformity of the graphene oxide layer decreases with the increasing treatment time. Since the 1 mg/mL and 2 mg/mL sensing layers' thicknesses were small and couldn't be measured using SEM, a gravimetric analysis of all our samples was carried out. Figure 6.b represents the variations of the GO-papers weight per area. The results show a positive linear relationship between the mass per area of the GO-coated paper and the treatment time, indicating an increase in the thickness of the deposited graphene oxide layer. The increase of the graphene oxide's thickness may be ascribed to the stacking of the graphene oxide sheets around the fibers which is enhanced by the high water absorbency coefficient of the paper (115 g/m^2).

3.2. Raman and Infrared spectroscopy

The fabricated sensors were characterized using FTIR and Raman spectroscopy (figure 7). Raman spectrum of the bare paper versus the Raman spectrum of a 4 mg/mL coated paper are shown in figures 7.a and 7.b. The spectrum of the coated paper exhibits two peaks at 1338 cm^{-1} and 1580 cm^{-1}. These two peaks are attributed to the D and G bands of the graphene oxide. Figure 7.c. plots the FTIR spectrums of bare paper and graphene oxide coated paper. FTIR spectrums shows a slight increase in the intensity the O-H peaks at 3300 cm^{-1} and 3265 cm^{-1}. This is mainly attributed to the remaining moisture inside the sensor. In fact, while graphene oxide sheets are being wrapped and stacked around the fibers, water molecules are stuck between the sheets, resulting in a shift in the O-H bond, and a slight increase in the intensity of its peak. The GO-paper spectrum also shows a small peak at 1750 cm^{-1} which is attributed to the formation of ester bonds between the paper and the sensing layer. The spectrum shows another peak at 1276 cm^{-1} attributed to the C-O stretching vibration of the ester bond. In order to explain this reaction, we should first note that viscose is the main chemical component of our substrate. Viscose molecules contain many hydroxyl functional groups (-OH). These groups will bond with the carbonyl functional groups (-COOH) of the graphene oxide to form a stable ester bond. A similar phenomenon is reported by J.-W. Han et al. describing the hydrogen bonding between carbon nanotubes and cellulosic paper [19, 40].

3.3. Mechanical strength and washability

In order to investigate the mechanical strength and the washability of the fabricated sensors, the sensors were washed and ultrasonicated in deionized water. The tests were performed on a 4 mg/mL GO-coated paper since changes are easier to spot with a scanning electron microscope for high concentrations of graphene oxide. As a result, 4 mg/mL GO-coated paper was cut into three pieces. The first piece served as a reference and was characterized using SEM (figure 8.a,b) and Raman spectroscopy (figure 9.a) . The second piece was washed in DI water for 10 minutes while stirring. The SEM images show little to no detachment of the graphene oxide coating around the fibers (figure 8.c,d). The Raman spectrums before and after immersing the sensor in water are similar, both with a D/G ratio of 0.98 (figure 9.b). The third piece of coated paper was ultrasonicated in a pulsed ultrasound bath for 5 minutes. The SEM images show a significant detachment of the graphene oxide sheets (figure 8.e,f). However, the resulting Raman spectrum is identical to the spectrums of the previous sample with two peaks at 1338 cm^{-1} and 1580 cm^{-1} and a D/G ratio of 0.98 (figure 9.c).

This highlights the fact that the fibers are still wrapped with graphene oxide and the fabricated sensors exhibit good mechanical strength and good hydrophobic properties. These results are consistent with the results obtained by W.Wu et al. regarding the hydrophobicity of graphene oxide wrapped around viscose fibers [43]. In fact, W.Wu et al. demonstrated that the water contact angle increased from 18˚ for bare viscose substrates to 119˚ for GO-coated viscose.

3.4. Electrical characterization

The conductivity of the sensing layer was characterized using a four-probe station. The I(V) characteristic of sensors with different concentrations of 1 mg/L, 2 mg/L and 4 mg/L of graphene oxide and different coating times (10 min, 30 min, 1 hour) are shown in figure 10. The curves show an increase in the conductivity of the sensing layer with the increasing concentration of graphene oxide and with the increasing immersion time. Moreover, the obtained characteristics are linear implicating the formation of ohmic contacts. However, only for low concentrations of graphene oxide (1 mg/mL) the conductivity of the sensing layer decreases with the increasing immersion time. This might be due to the non-uniformity of the deposited layer and to the increase of the water content inside the paper. Even though the conductivity of the graphene oxide wrapping decreases for low concentrations, the I(V) curves show an increase in their linearity and thus a better ohmic contact between the

IDEs and the GO-coated paper. Table 1 summarizes the resistances of the deposited graphene oxide layers calculated using the I(V) curves data points from figure 10.

3.5. Sensing performance

3.5.1. Sensing mechanism

The sensing mechanism between a carbon based material (CNTs, graphene and GO) and water molecules depends on the presence of hydrophilic functional groups on its surface such as hydroxyl groups. Graphene oxide is naturally functionalized with hydrophilic groups such as hydroxyl (-OH) and epoxy (=O) [44-48]. Upon its exposure to humidity, water molecules bind with the hydroxyl (-OH) and epoxy (=O) functional groups with binding energies of 0.201 and 0.259 eV respectively, thus withdrawing electrons from the graphene oxide [49]. As a result, graphene oxide becomes less conductive when exposed to a reducing gas such as water. Moreover, the viscose paper substrate used in this work contains hydroxyl functional groups. This makes our substrate sensitive towards humidity the same way. As a result, the paper substrate and the graphene oxide layer synergistically detect humidity.

3.5.2. Optimization of the deposited layer

The sensing performance of a gas sensor is evaluated based on its relative response towards a given analyte, its fast response, its fast recovery and its reversibility. The choice of the optimal gas sensor will be therefore based on these parameters. We first investigated the sensors' response towards 90% RH for an exposure time of 1 hour under ambient temperature. Then, the sensors recovered under 30% RH. The relative change in the capacitance of the fabricated devices were calculated and plotted for a frequency range of [0.5:200] kHz.

Since the weight per area of the sensors linearly increases with the processing time with almost the same slope (figure 6.b) for all concentrations of graphene oxide, the effect of the concentration of graphene oxide on the relative response of the fabricated sensors was investigated for a fixed immersion time of 10 minutes (figure 11.a.). The 2 mg/mL sensor exhibits the highest response towards humidity. This is mainly due to two factors: the porosity and the thickness of the GO layer wrapped around the paper's fibers. In fact, the 2 mg/mL sensor is porous and the 4 mg/mL sensor is not. This results in an increase of the contact surface between the active layer and the target molecules and explains the increased response of the 2 mg/mL sensor compared to the 4 mg/mL sensor. As for the 1 mg/mL sensor, the thickness/quantity of graphene oxide deposited onto the fibers is less than the one deposited using a 2 mg/mL suspension and the fibers weren't completely covered with graphene oxide. This limited the sensing capabilities of the sensor.

Figures 11.b, c and d show the effect of the treatment time on the response of the sensors. The relative change of the capacitance of the 1 mg/mL and 2 mg/mL sensors decrease with the increasing treatment time (figures 11.b., 11.c.). This is mainly due to the increase of the water content in the sensor, limiting thus the sensing capability of the device. In fact, the longer the sensor is immersed in the graphene oxide suspension, the more water molecules are stuck between the graphene oxide sheets and the more water is absorbed by the substrate. This phenomenon is enhanced by the high water absorbency coefficient of the paper. The trapped water molecules will interact with the functional groups of the graphene oxide and the paper substrate and thus will reduce the number of adsorption sites on the surface of the sensor. This results in a decrease of the sensitivity of the devices.

However, this is not the case of the 4 mg/mL sensors. The 4 mg/mL sensors plot (figure 11.d.) exhibits the highest relative response for a treatment time of 30 minutes. In fact, the relative response of the 4 mg/mL sensors increase with the increasing treatment time until it reaches a maximum for a treatment time of 30 min, then suddenly drops at 40 minutes. First, we must highlight that the 4 mg/mL sensors are not porous. The observed results may be explained as follows: the thickness of the graphene oxide layer increases with the increasing immersion time and so does the sensor's water content. Increasing the thickness up will result in an increase of the sensitivity of the sensor [50] while increasing the water content results in a decrease in the sensitivity of the

device (figures 11.b and 11.c). For a treatment time less than 30 minutes (<30 min), the thickness significantly increases with little effect on the sensing layer water content. As a result, the effect of the thickness will dominate the effect of the water content on the sensor's performance so the sensor's response increases. However, when the thickness of the graphene oxide layer exceeds a certain limit, the sensitivity of the graphene oxide layer towards humidity starts decreasing [51]. This is mainly due to the increase of the sensor's water content and to the fact that the sensing mechanism starts relying on bulk conductance changes instead of surface conductance changes. In fact, bulk conductance changes are slower and require more activation energy. As a result, the sensitivity of the GO-coated paper with a graphene oxide thickness exceeding 500 µm (figure 6.a.) starts decreasing.

In order to better optimize our device, we compared the sensing capabilities of the sensors that exhibit the best relative response for each concentration of graphene oxide, i.e., the 4 mg/mL - 30 min, 2 mg/mL - 10 min and 1 mg/mL - 10 min sensors. Based on the results shown in figure 12, the 4 mg/mL - 30 min sensor exhibits the highest response towards humidity. However, this sensor is not porous and has a slow response (5 min) and a 13% shift in its capacitance after recovery at 40 kHz (figure 12.b). Meanwhile, the 2 mg/mL - 10 min sensor is porous and exhibits the highest response towards humidity compared to the other porous sensors. Moreover, it detects humidity faster than the other sensors (3 min) and recovers with a 2% shift in its initial capacitance. For these reasons, the optimal graphene oxide concentration and immersion time are 2 mg/mL and 10 minutes, respectively.

3.6. 2mg/mL sensing response

a) Operating frequency

In order to better understand the frequency effect on the sensing capabilities of our devices, the relative response of both paper and GO-coated paper towards 90% RH were calculated and plotted for a frequency range of [0,5 : 200] kHz (figure 13). The results show that both paper and graphene oxide are sensitive towards humidity. For low frequencies (≤4 kHz), bare paper and GO-coated paper have comparable sensitivities towards humidity (~200%). However, for high frequencies (>4 kHz), the graphene oxide enhances the sensitivity of the paper by three times. This shows that functionalizing our paper with graphene oxide enables its use for high frequency applications. For these reasons, the optimal sensor will be tested at 40 kHz for the possibility of its use in RFID applications with an AMS chip (SL900).

b) Sensitivity and repeatability

The sensitivity and repeatability of the 2 mg/mL- 10 min sensor was tested under different relative humidity values. The sensor was exposed to the humidity for three consecutive cycles. Each cycle consists of the humidity step shown in figure 14.a. for three consecutive times. The relative response and the sensitivity of the 2 mg/mL sensor at 40 kHz are shown in figure 14.b.

The results show an increase in the capacitance of the device under humidity. The sensor exhibits a 38% relative response and a sensitivity of 5.65 fF/%RH at 40 kHz. The hysteresis of the device for different exposure cycles was also investigated (figure 15.a). The curves show an increase in the capacitance of the sensor by 0.02 pF after each exposure to humidity. This shift in the capacitance of the device is due to the slow desorption rate of the water molecules from the graphene oxide sensing layer. However, this capacitance shift did not affect the sensitivity (figure 16) and the hysteresis of the fabricated device (figure 15.b). In fact, the maximum hysteresis of 2.85% at 60% RH remained the same for all exposure cycles.

Table 2 summarizes the relative response and the sensitivity of the fabricated sensor for all exposure cycles. The relative response and the sensitivity of the device slightly decrease after the first exposure cycle and then stabilizes at the second exposure cycle. In conclusion, the 2 mg/mL (10 min) sensor exhibits a good response and repeatability at 40 kHz.

c) Flexibility

The flexibility of our device was tested for several values of the bending angle. The sensor was bent to 15˚, 30˚, 45˚, 60˚ and 75˚ using five small semi-cylinders fabricated by our team (figure 17). The sensor was afterwards exposed to a humidity step of 30% RH-90% RH.

The relative response (%) of the sensor was calculated and plotted (figure 18.a.). The results show a 10% decrease in the relative response the GO-coated paper after bending. However, the relative response is not affected by the magnitude of the bending angle. It has an average value of 31% and a standard deviation of 3.02. In order to further investigate the flexibility of our device, the ability of the sensor to be bent several times without any damage or performance loss was tested. The sensor's response was calculated at flat (0˚) and bent position (60˚) (Figure 18.b.). The results show that the relative response towards 90% RH decreases from 42% to 30% after bending the sensor for the first time. The response then stabilizes at 30% until the sensor saturated after bending the sensor for the third time. Heating the sensor at 50˚C for two days enabled a partial recovery of our device, which was able to detect humidity once again with a relative response of 20% at 60˚ bending angle. A possible explanation to this is that enlarging the pores while bending accelerated the saturation of the device and thus limited its sensibility towards humidity. We can conclude that the fabricated sensors are flexible and, once bended, their relative response no longer depends on the bending angle and the bending cycle, but only depends on the life expectancy of the device itself under ambient temperature.

d) Temperature effect

An interesting property of graphene oxide is its ability to detect humidity at room temperature. In order to further evaluate the effect of the temperature on the sensing capabilities of graphene oxide coated paper, the sensors were exposed to a humidity step of 50-90% RH for a temperature range of [15˚C:50˚C]. The response of the sensor under different values of the temperature is shown in figure 19 and summarized in table 3. The results don't show any effect of the operating temperature on the sensing capabilities of GO-coated paper. However, only for temperatures exceeding 50˚C, the desorption rate of the graphene oxide is enhanced (~0.4% capacitance shift instead of ~3%) with no effect on the relative response of the sensor. Heating the device at 50˚C increases thus the life expectancy of the GO-paper sensor with no effect on its response. This temperature independence is particularly interesting for applications in environments that require simple data acquisition and processing systems.

e) Stability

The stability of the fabricated sensors was tested under high relative humidity and at high temperature. Humidity sensing measurements were carried out under 90% RH humidity at ambient temperature. A first sensor (sensor 1), served as a reference and was characterized without any further treatment. Two other sensors (sensors 2 and 3) were placed in a climatic chamber under 85% RH at 50˚C. One of the sensors (sensor 2) was characterized at the end of the first week. The other (sensor 3) was characterized two weeks later. The sensors response towards 90% RH is plotted in figure 20. The sensors 1,2 and 3 exhibit a relative response of 34%, 37% and 32% respectively. Since the relative change in the sensitivity of our sensors is less than 5%, the sensor exhibits a good stability at high humidity and high temperature.

f) Reproducibility

The reproducibility of paper based graphene oxide humidity sensors using the proposed technique was tested as well. Ten gas sensors were exposed to 90% RH and recovered under 30% RH. The relative response of the sensors was calculated. The average response, the standard deviation and the standard error were calculated using the following formulas:

$$\overline{S_R} = \frac{\sum_{i=1}^{n} S_R}{n} \quad (4)$$

$$\sigma = \frac{\sum_{i=1}^{n}(S_{Ri} - \overline{S_R})^2}{n} \quad (5)$$

$$\sigma_{\overline{S_R}} = \frac{\sigma}{\sqrt{n}} \quad (6)$$

The sensors exhibit an average response of 38% towards 90% RH with a standard deviation of 2,14 and a standard error of 0,68. Since the standard error is less than 1, the proposed fabrication technique is thus considered reproducible and reliable for the large scale production of low cost devices. Table 4 summarizes all flexible porous paper-based gas sensors and all flexible graphene oxide based humidity sensors reported in the literature. This table compares their sensing properties to the properties of the sensor reported in this paper.

Even though humidity sensors based on, or functionalized by metal oxide nanostructures and TDMCs on plastic substrates have better sensing performance in terms of sensitivity [16, 18, 20, 21] (table 4), the sensors reported in this work have several advantages in terms of flexibility, application fields and biodegradability. The sensors reported in this work are highly porous and ideal for air flow monitoring in both directions. Moreover, the fabricated sensors are washable, highly flexible and ideal for e-dressings and e-textiles. These applications cannot be covered using plastic substrates without any damage to the device. Ecologically, this work presents a green alternative for plastic substrates, metal oxides, polymers and TDMCs. In addition to the biodegradability of paper, the biodegradation of graphene oxide by microbes and enzymes has been reported [52, 53]. As a result, the proposed approach contributes to the reduction of electronic plastic and chemical waste and thus to the reduction of soil and water pollution. Last, from a technical point of view, the proposed sensors are highly flexible. Most sensors found in the literature weren't tested under strain, or their response decreased with the increasing bending angle. In this work, the sensors' response becomes independent of the bending angle and the bending cycle after bending the device for the first time. Last, our work enables the use of porous paper substrates for capacitive humidity sensing at high frequencies, with a relative response comparable to the resistive cellulosic paper-based sensors found in the literature.

4. Conclusion

This paper reports the fabrication of a flexible humidity sensor by integrating a graphene oxide sensing layer in a porous paper substrate using a simple self-assembly technique. The effect of the thickness, porosity and moisture content on the humidity sensing performance of the GO-paper as a function of the frequency was investigated. Immersing the paper in a 2 mg/mL graphene oxide suspension for 10 min gave the best results in terms of porosity, relative response, response and recovery time. Moreover, graphene oxide, as a sensing element, increased the sensibility of paper by three times at 40 kHz, enabling thus its use in RFID applications. The optimal sensor exhibits a good sensing response (38%) towards 90% RH, a good repeatability, long term stability and reproducibility at 40 kHz. The fabricated sensor is highly flexible: its relative response becomes independent of the bending angle and of the bending cycle after bending the sensor for the first time. However, the performance of GO-coated paper is limited by its slow recovery, which required heating the sensor at 50˚C. An operating temperature of 50˚C speeded the recovery of the GO-paper without affecting its response towards humidity. In summary, the simple low cost fabrication technique proposed in this work combines the advantages of paper based electronics with those of e-textiles, covering thus a wide range of applications such as smart packaging, e-dressings, e-textiles, and even air flow monitoring.

Acknowledgments

The authors would like to acknowledge the National Council for Scientific Research of Lebanon (CNRS-L), the University of Montpellier (UM) and the 'Agence Universitaire de la Francophonie' (AUF) for granting a doctoral fellowship to Rouba Alrammouz. The author Roland Habchi would like to thank the scientific research program of the Lebanese University for the research grant.

References

[1] H. Farahani, R. Wagiran, and M. Hamidon, "Humidity Sensors Principle, Mechanism, and Fabrication Technologies: A Comprehensive Review," *Sensors,* vol. 14, no. 5, p. 7881, 2014.

[2] A. Arena, N. Donato, and G. Saitta, "Capacitive humidity sensors based on MWCNTs/polyelectrolyte interfaces deposited on flexible substrates," *Microelectronics Journal,* vol. 40, no. 6, pp. 887-890, 2009.

[3] A. Oprea, J. Courbat, N. Bârsan, D. Briand, N. F. de Rooij, and U. Weimar, "Temperature, humidity and gas sensors integrated on plastic foil for low power applications," *Sensors and Actuators B: Chemical,* vol. 140, no. 1, pp. 227-232, 2009.

[4] A. S. G. Reddy, B. B. Narakathu, M. Z. Atashbar, M. Rebros, E. Rebrosova, B. J. Bazuin, M. K. Joyce, P.D. Fleming, and A. Pekarovicova, "Printed Capacitive Based Humidity Sensors on Flexible Substrates," *Sensor Letters,* vol. 9, no. 2, pp. 869-871, 2011.

[5] A. S. G. Reddy, B. B. Narakathu, M. Z. Atashbar, M. Rebros, E. Rebrosova, and M. K. Joyce, "Fully Printed Flexible Humidity Sensor," *Procedia Engineering,* vol. 25, pp. 120-123, 2011.

[6] E. Zampetti, S. Pantalei, A. Pecora, A. Valletta, L. Maiolo, A. Minotti, A. Macagnano, G. Fortunato, and A. Bearzotti, "Design and optimization of an ultra thin flexible capacitive humidity sensor," *Sensors and Actuators B: Chemical,* vol. 143, no. 1, pp. 302-307, 2009.

[7] G. Mattana, T. Kinkeldei, D. Leuenberger, C. Ataman, J. J. Ruan, F. Molina-Lopez, A. V. Quintero, G. Nisato, G. Tröster, and D. Briand, "Woven temperature and humidity sensors on flexible plastic substrates for e-textile applications," *IEEE Sensors Journal,* vol. 13, no. 10, pp. 3901-3909, 2013.

[8] J. Pelegri-Sebastia, E. Garcia-Breijo, J. Ibanez, T. Sogorb, N. Laguarda-Miro, and J. Garrigues, "Low-Cost Capacitive Humidity Sensor for Application Within Flexible RFID Labels Based on Microcontroller Systems," *IEEE Transactions on Instrumentation and Measurement,* vol. 61, no. 2, pp. 545-553, 2012.

[9] P.M. Harrey, B. J. Ramsey, P. S. A. Evans, and D. J. Harrison, "Capacitive-type humidity sensors fabricated using the offset lithographic printing process," *Sensors and Actuators B: Chemical,* vol. 87, no. 2, pp. 226-232, 2002.

[10] T. Yang, Y. Z. Yu, L. S. Zhu, X. Wu, X. H. Wang, and J. Zhang, "Fabrication of silver interdigitated electrodes on polyimide films via surface modification and ion-exchange technique and its flexible humidity sensor application," *Sensors and Actuators B: Chemical,* vol. 208, pp. 327-333, 2015/03/01/ 2015.

[11] U. Altenberend, F. Molina-Lopez, A. Oprea, D. Briand, N. Bârsan, N. De Rooij, and U. Weimar, "Towards fully printed capacitive gas sensors on flexible PET substrates based on Ag interdigitated transducers with increased stability," *Sensors and Actuators B: Chemical,* vol. 187, pp. 280-287, 2013/10/01/ 2013.

[12] C. Vaghela, M. Kulkarni, S. Haram, M. Karve, and R. Aiyer, "Biopolymer-Polyaniline Composite for a Wide Range Ammonia Gas Sensor," *IEEE Sensors Journal,* vol. 16, no. 11, pp. 4318-4325, 2016.

[13] F. Bibi, C. Guillaume, B. Sorli, and N. Gontard, "Plant polymer as sensing material: Exploring environmental sensitivity of dielectric properties using interdigital capacitors at ultra high frequency," *Sensors and Actuators B: Chemical,* vol. 230, pp. 212-222, 2016.

[14] F. Bibi, C. Guillaume, N. Gontard, and B. Sorli, "Wheat gluten, a bio-polymer to monitor carbon dioxide in food packaging: Electric and dielectric characterization," *Sensors and Actuators B: Chemical,* vol. 250, pp. 76-84, 2017.

[15] N. Gontard, R. Thibault, B. Cuq, and S. Guilbert, "Influence of Relative Humidity and Film Composition on Oxygen and Carbon Dioxide Permeabilities of Edible Films," *Journal of Agricultural and Food Chemistry,* vol. 44, no. 4, pp. 1064-1069, 1996/01/01 1996.

[16] M. Balde, A. Vena, and B. Sorli, "Fabrication of porous anodic aluminium oxide layers on paper for humidity sensors," *Sensors and Actuators B: Chemical,* vol. 220, pp. 829-839, 2015.

[17] T. Islam, M. R. Mahboob, and S. A. Khan, "A Simple MOX Vapor Sensor on Polyimide Substrate for Measuring Humidity in ppm Level," *IEEE Sensors Journal,* vol. 15, no. 5, pp. 3004-3013, 2015.

[18] D. Zhang, X. Zong, Z. Wu, and Y. Zhang, "Hierarchical Self-Assembled SnS2 Nanoflower/Zn2SnO4 Hollow Sphere Nanohybrid for Humidity-Sensing Applications," *ACS Applied Materials & Interfaces,* vol. 10, no. 38, pp. 32631-32639, 2018/09/26 2018.

[19] J.-W. Han, B. Kim, J. Li, and M. Meyyappan, "Carbon Nanotube Based Humidity Sensor on Cellulose Paper," *The Journal of Physical Chemistry C,* vol. 116, no. 41, pp. 22094-22097, 2012.

[20] D. Zhang, X. Zong, and Z. Wu, "Fabrication of tin disulfide/graphene oxide nanoflower on flexible substrate for ultrasensitive humidity sensing with ultralow hysteresis and good reversibility," *Sensors and Actuators B: Chemical,* vol. 287, pp. 398-407, 2019/05/15/ 2019.

[21] D. Zhang, Y. Sun, P. Li, and Y. Zhang, "Facile Fabrication of MoS2-Modified SnO2 Hybrid Nanocomposite for Ultrasensitive Humidity Sensing," *ACS Applied Materials & Interfaces,* vol. 8, no. 22, pp. 14142-14149, 2016/06/08 2016.

[22] J. Courbat, Y. B. Kim, D. Briand, and N. F. d. Rooij, "Inkjet printing on paper for the realization of humidity and temperature sensors," in *16th International Solid-State Sensors, Actuators and Microsystems Conference*, 2011, pp. 1356-1359.

[23] A. Kafy, A. Akther, M. I. R. Shishir, H. C. Kim, Y. Yun, and J. Kim, "Cellulose nanocrystal/graphene oxide composite film as humidity sensor," *Sensors and Actuators A: Physical,* vol. 247, pp. 221-226, 2016.

[24] C. Lee, J. Ahn, K. B. Lee, D. Kim, and J. Kim, "Graphene-based flexible NO2 chemical sensors," *Thin Solid Films,* vol. 520, no. 16, pp. 5459–5462, 2012.

[25] G. Yang, C. Lee, J. Kim, F. Ren, and S. J. Pearton, "Flexible graphene-based chemical sensors on paper substrates," *Physical Chemistry Chemical Physics,* vol. 15, no. 6, pp. 1798--1801, 2013.

[26] K. Toda, R. Furue, and S. Hayami, "Recent progress in applications of graphene oxide for gas sensing: A review," *Analytica Chimica Acta,* vol. 878, pp. 43-53, 2015.

[27] D. Zhang, H. Chang, P. Li, R. Liu, and Q. Xue, "Fabrication and characterization of an ultrasensitive humidity sensor based on metal oxide/graphene hybrid nanocomposite," *Sensors and Actuators B: Chemical,* vol. 225, pp. 233-240, 2016.

[28] D. Zhang, J. Liu, and B. Xia, "Layer-by-Layer Self-Assembly of Zinc Oxide/Graphene Oxide Hybrid Toward Ultrasensitive Humidity Sensing," *IEEE Electron Device Letters,* vol. 37, no. 7, pp. 916-919, 2016.

[29] D. Zhang, J. Tong, B. Xia, and Q. Xue, "Ultrahigh performance humidity sensor based on layer-by-layer self-assembly of graphene oxide/polyelectrolyte nanocomposite film," *Sensors and Actuators B: Chemical,* vol. 203, pp. 263-270, 2014.

[30] H. Bi, K. Yin, X. Xie, J. Ji, S. Wan, L. Sun, M. Terrones, and M. S. Dresselhaus, "Ultrahigh humidity sensitivity of graphene oxide," *Scientific Reports,* Article vol. 3, p. 2714, 09/19/online 2013.

[31] S. Ali, A. Hassan, G. Hassan, J. Bae, and C. H. Lee, "All-printed humidity sensor based on graphene/methyl-red composite with high sensitivity," *Carbon,* vol. 105, pp. 23-32, 2016.

[32] B. Wu, X. Zhang, B. Huang, Y. Zhao, C. Cheng, and H. Chen, "High-Performance wireless amonia gas sensors based on reduced graphene oxide and nano-silver ink hybrid material loaded on a patch antenna," *Sensors,* vol. 17, no. 9, p. 2070, 2017.

[33] D. Zhang, J. Tong, and B. Xia, "Humidity-sensing properties of chemically reduced grapheneoxide/polymer nanocomposite film sensor based on layer-by-layernano self-assembly," *Sensors and Actuators B: Chemical,* vol. 197, pp. 66-72, 2014.

[34] H. Y. Jeong, D.-S. Lee, H. K. Choi, D. H. Lee, J.-E. Kim, J. Y. Lee, W. J. Lee, S. O. Kim, and S.-Y. Choi, "Flexible room-temperature NO 2 gas sensors based on carbon nanotubes/reduced graphene hybrid films," *Applied Physics Letters,* vol. 96, no. 21, p. 213105, 2010.

[35] L. Huang, Z. Wang, J. Zhang, J. Pu, S. X. Y. Lin, L. Shen, Q. Chen, and W. Shi, "Fully printed, rapid-response sensors based on chemically modified graphene for detecting NO2 at room temperature," *ACS Applied Materials and interfaces,* vol. 6, no. 10, p. 7426−7433, 2014.

[36] P.-G. Su and H.-C. Shieh, "Flexible NO2 sensors fabricated by layer-by-layer covalent anchoring and in situ reduction of graphene oxide," *Sensors and Actuators B: Chemical,* vol. 190, pp. 865– 872, 2014.

[37] S. M. Shumao Cui, Zhenhai Wen, Jingbo Chang, Yang Zhang, Junhong Chen, "Controllable synthesis of silver nanoparticle-decorated reduced graphene oxide hybrids for ammonia detection," *Analyst,* vol. 138, pp. 2877–2882, 2013.

[38] V. Dua, S. P. Surwade, S. Ammu, S. R. Agnihotra, S. Jain, K. E. Roberts, S. Park, R. S. Ruoff, and S. K. Manohar, "All-Organic vapor sensor using inkjet-printed reduced graphene oxide," *Angewandte Chemie International Edition,* vol. 49, no. 12, pp. 2154–2157, 2010.

[39] N. H. Xiaolu Huang, Liling Zhang, Liangming Wei, Hao Wei, Yafei Zhang, "The NH3 sensing properties of gas sensors based on aniline reduced graphene oxide," *Synthetic Metals,* vol. 185-186, pp. 25– 30, 2013

[40] J.-W. Han, B. Kim, J. Li, and M. Meyyappan, "A carbon nanotube based ammonia sensor on cellulose paper," *RSC Advances,* vol. 4, no. 2, pp. 549-553, 2014.

[41] S.Ammu, V. Dua, S.-R. Agnihotra, S. P. Surwade, A. Phulgirkar, S. Patel, and S. K. Manohar, "Flexible, all-organic chemiresistor for detecting chemically aggressive vapors," *Journal of the American Chemical Society,* vol. 134, no. 10, pp. 4553-4556, 2012.

[42] R. P. Gandhiraman, E. Singh, D. C. Diaz-Cartagena, D. Nordlund, J. Koehne, and M. Meyyappan, "Plasma jet printing for flexible substrates," *Applied Physics Letters,* vol. 108, no. 12, p. 123103, 2016.

[43] H. Z. W. Wu, H. Ma, J. Cao, L. Jiang, G. Chen, "Functional finishing of viscose knitted fabrics via graphene coating," *Journal of Engineered fibers and fabrics,* vol. 12, no. 3, 2017.

[44] A. Lerf, H. He, M. Forster, and J. Klinowski, "Structure of Graphite Oxide Revisited," *The Journal of Physical Chemistry B,* vol. 102, no. 23, pp. 4477-4482, 1998.

[45] D. Dreyer, S. Park, C. Bielawski, and R. Ruoff, "The chemistry of graphene oxide," *Chemical Society Reviews,* vol. 39, no. 1, pp. 228–240, 2010.

[46] G. Ruess, "Über das Graphitoxyhydroxyd (Graphitoxyd)," *Monatshefte für Chemie und verwandte Teile anderer Wissenschaften,* vol. 76, no. 3-5, pp. 381-417, 1947.

[47] U. Hofmann and R. Holst, "Über die Säurenatur und die Methylierung von Graphitoxyd," *Berichte der deutschen chemischen Gesellschaft (A and B Series),* vol. 72, no. 4, pp. 754-771, 1939.

[48] W. Scholz and H. P. Boehm, "Untersuchungen am Graphitoxid. VI. Betrachtungen zur Struktur des Graphitoxids," *Zeitschrift für anorganische und allgemeine Chemie,* vol. 369, no. 3-6, pp. 327-340, 1969.

[49] L. Guo, H. B. Jiang, R. Q. Shao, Y. L. Zhang, S. Y. Xie, J. N. Wang, X. B. Li, F. Jiang, Q. D. Chen, T. Zhang, and H. B. Sun, "Two-beam-laser interference mediated reduction, patterning and nanostructuring of graphene oxide for the production of a flexible humidity sensing device," *Carbon,* vol. 50, no. 4, pp. 1667-1673, 2012.

[50] Y. Zhou, Y. Jiang, T. Xie, H. Tai, and G. Xie, "A novel sensing mechanism for resistive gas sensors based on layered reduced graphene oxide thin films at room temperature," *Sensors and Actuators B: Chemical,* vol. 203, pp. 135-142, 2014/11/01/ 2014.

[51] S. Papamatthaiou, D. P. Argyropoulos, F. Farmakis, A. Masurkar, K. Alexandrou, I. Kymissis, and N. Georgoulas, "The Effect of Thermal Reduction and Film Thickness on fast Response Transparent Graphene Oxide Humidity Sensors," *Procedia Engineering,* vol. 168, pp. 301-304, 2016/01/01/ 2016.

[52] M. Chen, X. Qin, and G. Zeng, "Biodegradation of carbon nanotubes, graphene, and their derivatives," *Trends in biotechnology,* vol. 35, no. 9, pp. 836-846, 2017.

[53] R. Kurapati, J. Russier, M. A. Squillaci, E. Treossi, C. Ménard-Moyon, A. E. Del Rio-Castillo, E. Vazquez, P. Samorì, V. Palermo, and A. Bianco, "Dispersibility-dependent biodegradation of graphene oxide by myeloperoxidase," *Small,* vol. 11, no. 32, pp. 3985-3994, 2015.

[54] P.-G. Su, W.-L. Shiu, and M.-S. Tsai, "Flexible humidity sensor based on Au nanoparticles/graphene oxide/thiolated silica sol–gel film," *Sensors and Actuators B: Chemical,* vol. 216, pp. 467-475, 2015/09/01/ 2015.

[55] P.-G. Su and Z.-M. Lu, "Flexibility and electrical and humidity-sensing properties of diamine-functionalized graphene oxide films," *Sensors and Actuators B: Chemical,* vol. 211, pp. 157-163, 2015/05/01/ 2015.

Tables captions

Table 1. Resistance of the graphene oxide layer in MΩ.

Table 2. Relative response and sensitivity of the optimal sensor as a function of the exposure cycle.

Table 3. Relative response and capacitance shift after desorption of the optimal sensor at different temperatures.

Table 4. Porous paper-based gas sensors and graphene oxide based humidity sensors reported in the literature.

Figures captions

Figure 1. (a) Deposition technique **(b)** Dimensions of the interdigitated electrodes in millimeters **(c)** 2 mg/mL - 10 min sensor.

Figure 2. (a) Two probe testing device **(b)** Gas sensing test bench.

Figure 3. SEM images **(a)** paper **(b)** 1 mg/mL GO **(c)** 2 mg/mL GO **(d)** 4 mg/mL GO.

Figure 4. SEM images of a 4 mg/mL GO coating with an immersion time of **(a)** 10 min **(b)** 30 min **(c)** 1 hour.

Figure 5. SEM images showing the thickness of paper immersed in 4 mg/mL GO suspension for **(a)** 10 min **(b)** 30 min **(c)** 60 min.

Figure 6. (a) Thickness of GO-paper as a function of the processing time in a 4 mg/mL graphene oxide suspension **(b)** Gravimetric measurements of GO-coated papers for different processing times in different concentrations of graphene oxide.

Figure 7. (a) Raman spectrum of bare paper **(b)** Raman spectrum of GO coated paper **(c)** FTIR spectrums of bare paper and GO-coated paper.

Figure 8. SEM images **(a,b)** before washing treatment **(c,d)** after washing treatment **(e,f)** after ultrasonication.

Figure 9. Raman spectrums of the sensor **(a)** before **(b)** after water treatment **(c)** after ultrasonication.

Figure 10. I(V) curves of **(a)** 1 mg/mL **(b)** 2 mg/mL **(c)** 4 mg/mL sensors with different immersion times (10 min, 30 min, 60 min).

Figure 11. Relative response of GO-coated paper as a function of the frequency and **(a)** of the concentration of graphene oxide **(b)** treatment time for a GO concentration of 1 mg/mL **(c)** treatment time for a GO concentration of 2 mg/mL **(d)** treatment time for a GO concentration of 4 mg/mL.

Figure 12. Relative response of the 4 mg/mL – 30 min, 2 mg/mL – 10 min and 1 mg/mL – 10 min as a function of **(a)** the frequency **(b)** the time at 40 kHz.

Figure 13. Relative response of bare paper versus the relative response of GO-coated paper towards 90% RH as a function of the frequency.

Figure 14. (a) humidity step **(b)** Real time relative humidity in the climatic chamber.

Figure 15. (a) Hysteresis for the first exposure cycle **(b)** Capacitance shift as a function of the relative humidity and the exposure cycle.

Figure 16. Sensitivity curve as a function of the exposure cycle.

Figure 17. Flexibility measurement setup.

Figure 18. Relative response (%) as a function of **(a)** the bending angle **(b)** the bending cycle.

Figure 19. Temperature effect on the sensing response of the 2 mg/mL – 10 min GO-coated paper.

Figure 20. Stability under 85% RH at 50˚C.

Biographies

Rouba Alrammouz received her diploma in Electrical and Electronics Engineering in 2015 from the Lebanese University – Faculty of Engineering, Lebanon. In 2016, she obtained the M.S degree in microsystems and embedded systems from the Lebanese University – Faculty of Sciences, Lebanon. She is currently a joint Ph.D. student at the Institute of Electronics (IES), University of Montpellier, France, and at the EC2M lab, Lebanese University, Lebanon. Her areas of research interest include capacitive sensors, graphene-based gas sensors and paper based flexible and wearable electronics.

Jean PODLECKI received his Ph.D. in electronics optronics and systems from the university of Montpellier, France, in 1995. After a stay at LIMMS, CNRS laboratory based in Japan, he worked in the field of MEMS and MOEMS and was involved in different startups. Since 2004, he works at the University of Montpellier at the Institute of Electronics (IES, UMR5214), first on the study of thermoelectric materials and their application to fast micro and nano thermique and now on the study and realization of graphene oxide based sensor on flexible substrate (in the RFID and flexible electronics group).

Dr. Arnaud Vena received the Eng. Dipl. Degree in electrical engineering from Institut National Polytechnique de Grenoble (Grenoble-INP), Grenoble, France, in 2005, and the Ph.D. degree from Université de Grenoble, Grenoble, in 2012. In 2005, he joined ACS Solution France SAS and was responsible for the development of radio frequency identification (RFID) contactless card readers. In October 2009, he started his research within Grenoble-INP, focused on the design of chipless RFID systems. From 2012-2013 he held a postdoctoral position at the Tampere University of Technology in Finland, in the field of conventional and chipless RFID sensors. Since September 2013, he is an associate professor in electrical engineering at Université de Montpellier within the IES lab. His current research interests are in the field of wireless sensors, RFID systems and printed electronics.

Ricardo GARCIA received the degrees of BSc and BEng in Electrical and Electronics Engineering from the University of Barcelona in 1995. After he integrated the industry where he has worked for different companies Fujitsu, Siemens, Hewlett Packard, etc. in the R&D sector the microelectronics systems. In France received the M.S. and Ph.D. degrees in electrical engineering from the University of Perpignan and University of Montpellier, in 2011 and 2014, respectively. During this period, he worked on the study and realization of energy micro-sources and graphene oxide based supercapacitors, for use in autonomous wireless sensor networks and integration on a flexible substrate. Since 2014, he works at the University of Montpellier at the Institute of Electronics (IES, UMR5214), his research interests focus on flexible sensors, micro-energy harvesting, integrated power management, and ultra-low-power interface circuit for sensors design.

Pascale Abboud obtained her M.S in nanoscience and functional materials (2010) from the Lebanese University and received her Ph.D. (2014) in physics from Université de Montpellier. She joined EC2M at the Lebanese University (2014) and is currently a lecturer at Université Saint-Joseph de Beyrouth. Her research interests include characterization of electronic transport in microcrystalline silicon and graphene-oxide based gas sensors.

Prof. Roland Habchi received his Ph.D. degree in microelectronics from the University of Perpignan Via Domitia in 2007. He became an associate professor of physics at the Lebanese University, Faculty of Sciences 2 and then a full-time professor in 2013. In 2012, he helped installing the Research Platform for Nanoscience and

Nanotechnology and is still handling the research activities in this platform. In 2016, he created a new research laboratory called EC2M, gathering researchers from all departments of the faculty of science. His research is mainly focused on experimental aspects of materials science and smart nanostructures (physical vapor deposition, atomic layer deposition, plasma enhanced chemical vapor deposition, magnetic materials, sensors, and detectors) and theoretical aspects of solid-state physics. Since 2012, he has served as a member of the scientific board of the Research Platform for Nanoscience and Nanotechnology.

Dr. Brice Sorli (Associate Professor) received the M.S degree Applied Physics and Ph.D degree in Electrical Engineering from Montpellier University in 1998 and 2001, respectively. During this period, he worked on electronic measurements, instrumentation, thermal analysis and humidity sensors. In 2002, he joined the "Electronic, Nanotechnologies & Sensors Lab" (INL), Claude Bernard University, Lyon where he has been involved in the design and implementation of nuclear magnetic resonance micro-probe for « Labs on chip » and in vivo applications. Since 2005, he works at the "Electronic Institute Lab" (IES), Montpellier University, on flexible sensors and RFID applications.

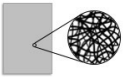

Paper substrate
2 cm x 2 cm – 25 g/m^2 –
102 µm

Immersion

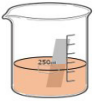

Self-
assembly

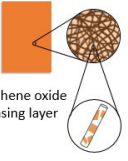

Graphene oxide
sensing layer

Thermal
evaporation

Aluminum interdigitated
electrodes – 500 nm

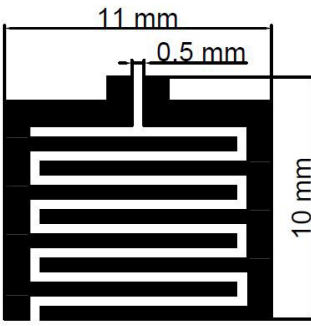
11 mm
0.5 mm
10 mm

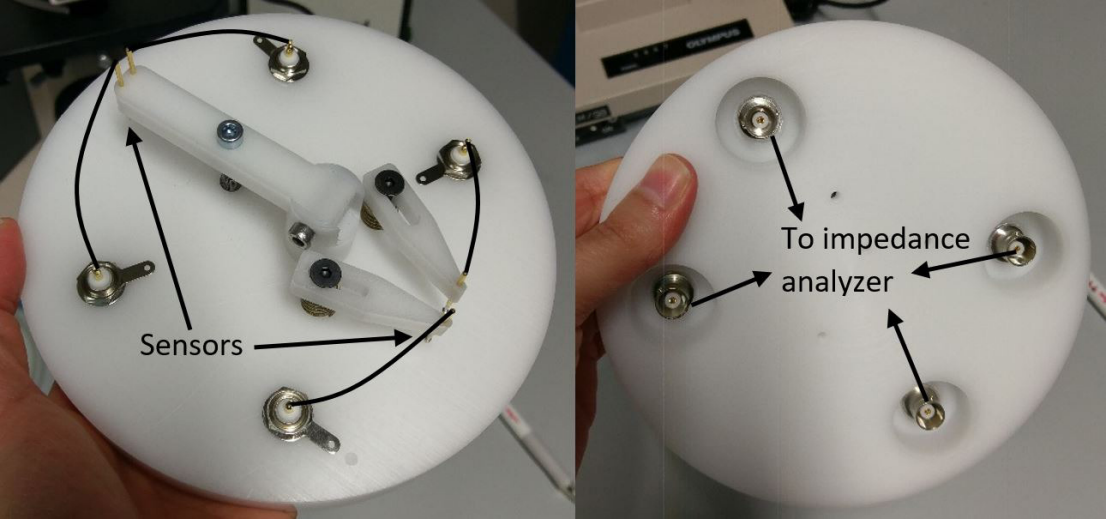
Sensors
To impedance
analyzer


espec
SH-242
Bench-top Type
Temperature & Humidity Chamber
22.0 °C
32 %rh
GREEN PRODUCT
4192A LF IMPEDANCE ANALYZER
HEWLETT-PACKARD
DISPLAY A
DISPLAY B
1.5077
0.316
198.0000
OEN 868
CAUTION
APPLYING EXCESSIVE DC VOLTAGE TO THE UNKNOWN
TERMINALS WILL DAMAGE THE INSTRUMENT. FOR DETAILS
REFER TO "WILL DAMAGE THE INSTRUMENT" SECTION IN
GIVEN IN THE MANUAL
UNKNOWN
DELL

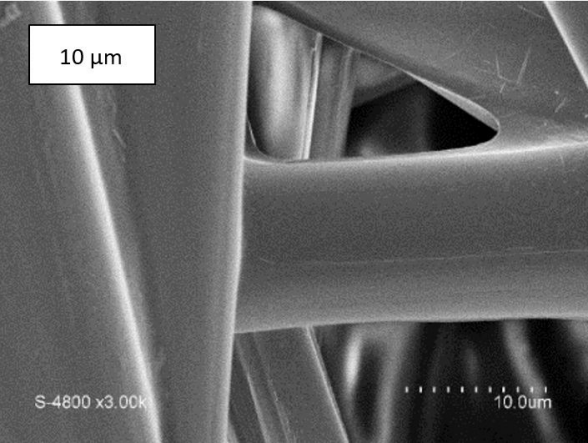
10 µm
S-4800 x3.00k
10.0um

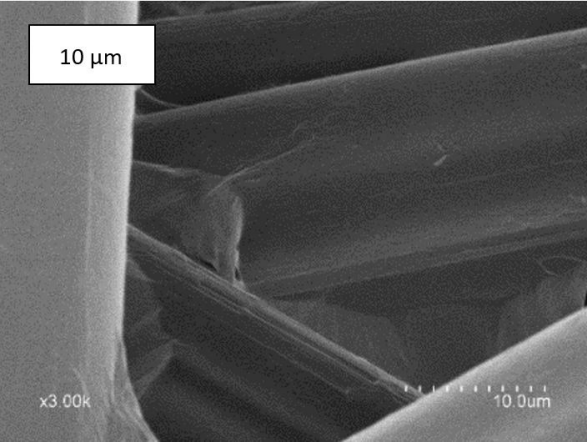
10 µm
x3.00k
10.0um

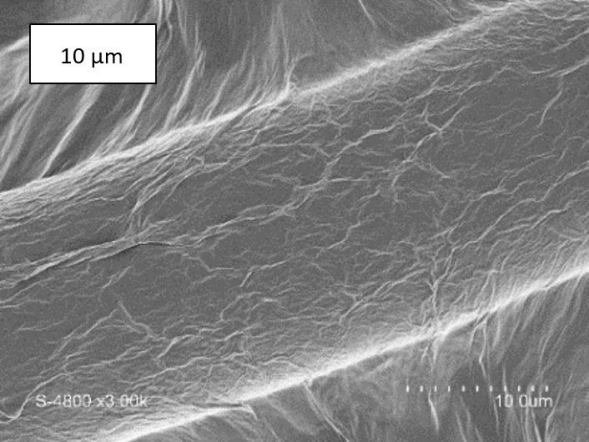
10 µm
S-4800 x3.00k
10.0um

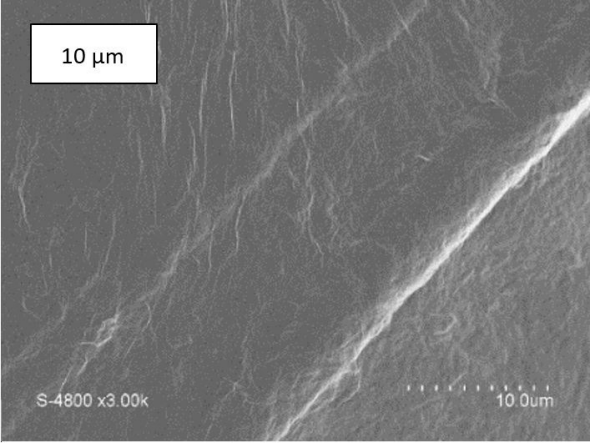
10 µm
S-4800 x3.00k
10.0um

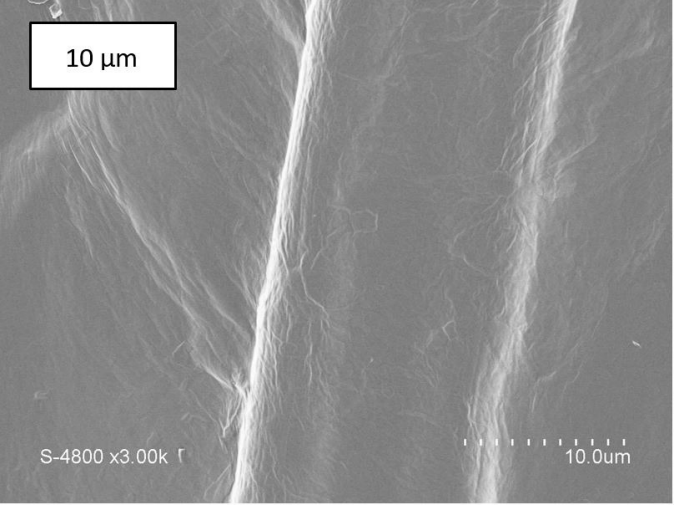
10 µm
S-4800 x3.00k
10.0um

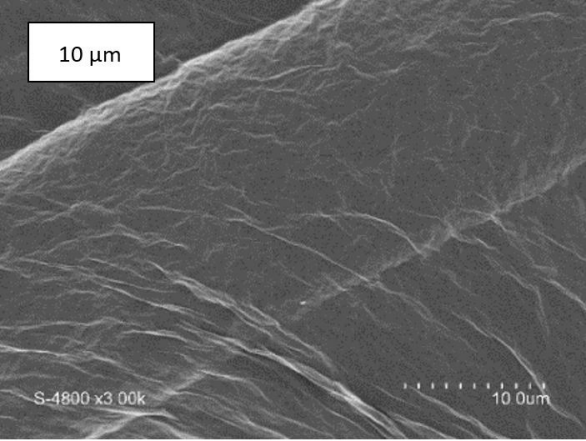
10 µm
S-4800 x3 00k
10 0um

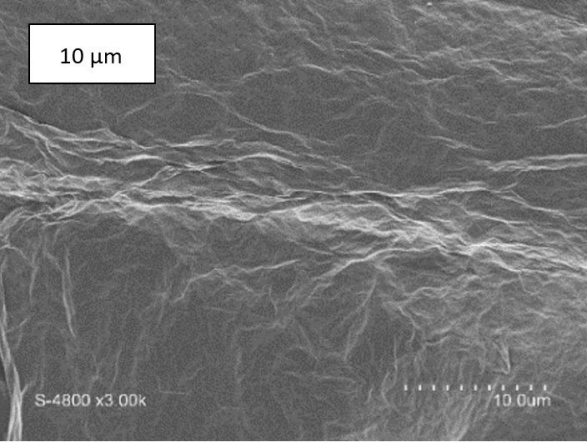
10 µm
S-4800 x3.00k
10.0um

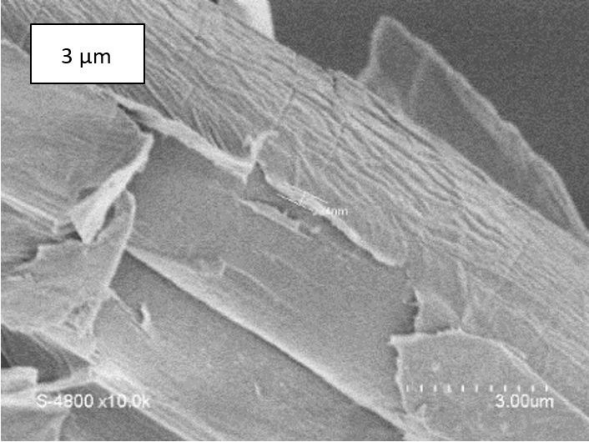
3 µm
S-4800 x10.0k
3.00um

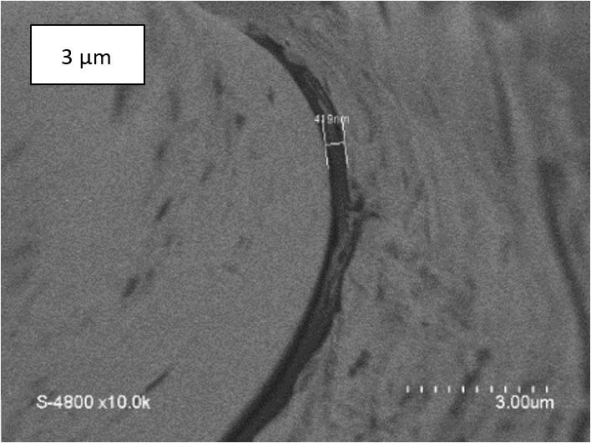
3 µm
S-4800 x10.0k
3.00um

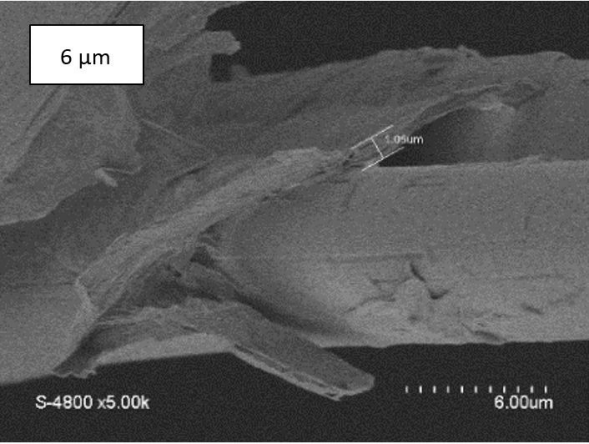
6 µm
1.05um
S-4800 x5.00k
6.00um

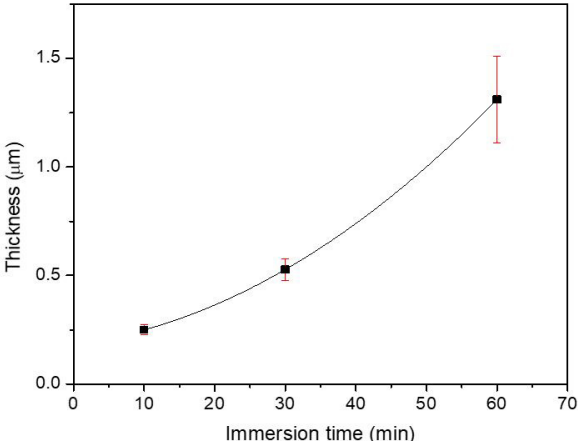
Thickness (μm)
0.0
0.5
1.0
1.5
0
10
20
30
40
50
60
70
Immersion time (min)

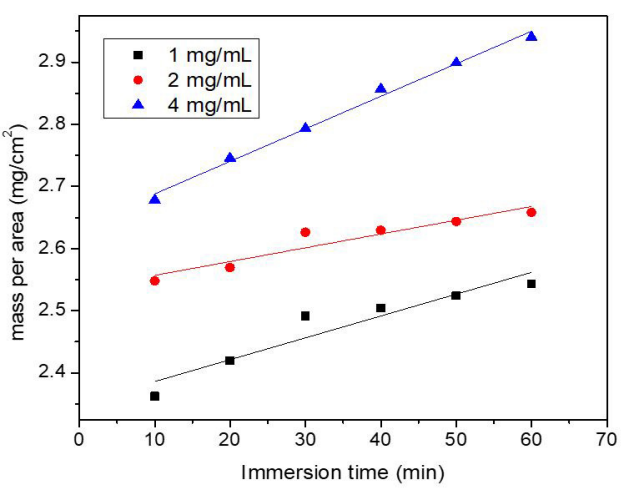
1 mg/mL
2 mg/mL
4 mg/mL
mass per area (mg/cm2)
Immersion time (min)
2.4
2.5
2.6
2.7
2.8
2.9
0
10
20
30
40
50
60
70

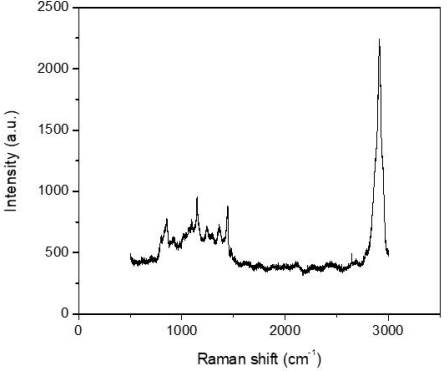
2500
2000
1500
1000
500
0
Intensity (a.u.)
0
1000
2000
3000
Raman shift (cm-1)

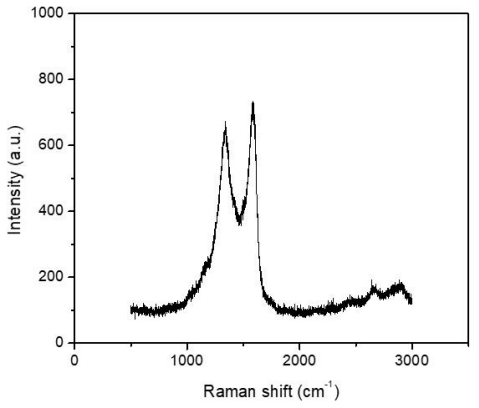
1000
800
600
400
200
0
Intensity (a.u.)
0
1000
2000
3000
Raman shift (cm-1)

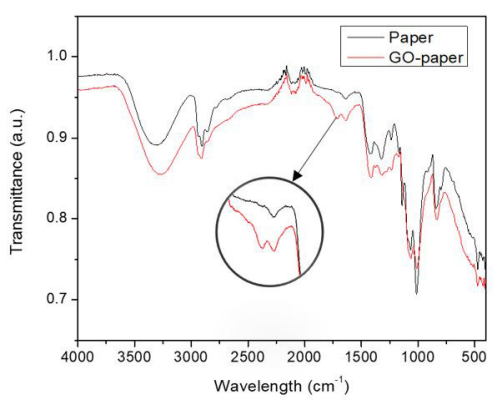
Paper
GO-paper
Transmittance (a.u.)
1.0
0.9
0.8
0.7
4000
3500
3000
2500
2000
1500
1000
500
Wavelength (cm-1)

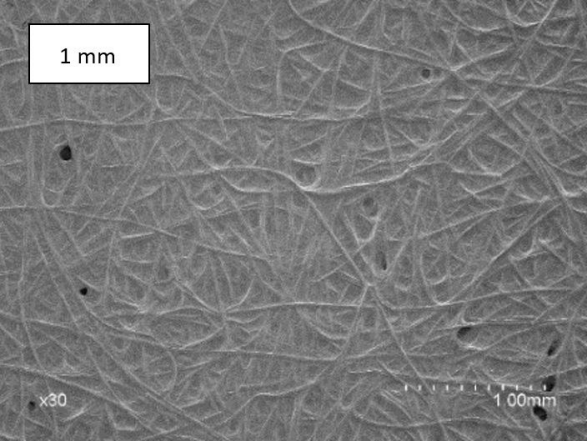
1 mm
x30
1.00mm

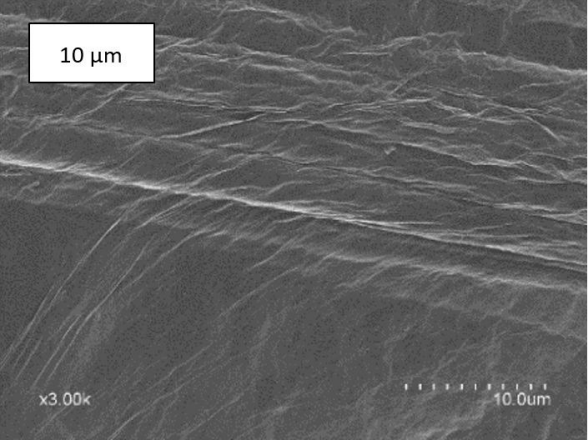
10 µm
x3.00k
10.0um

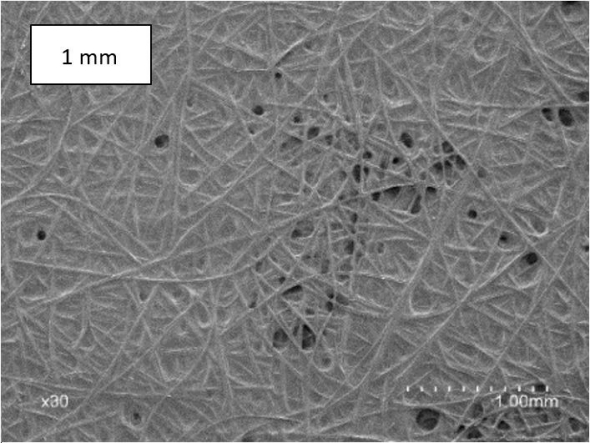
1 mm
x30
1.00mm

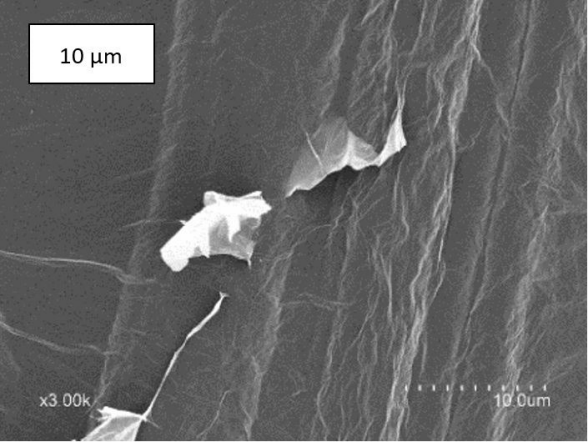
10 µm
x3.00k
10.0um

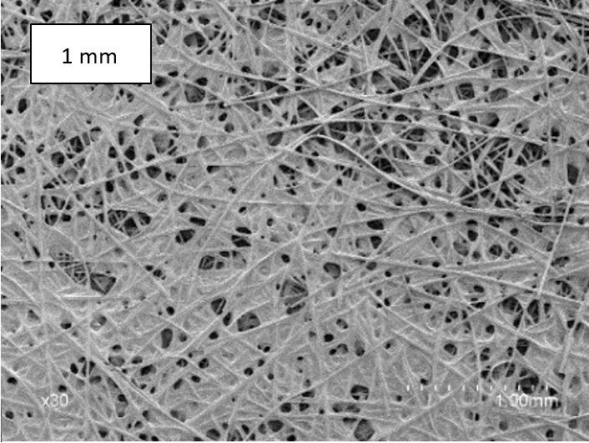
1 mm
x20
1.00mm

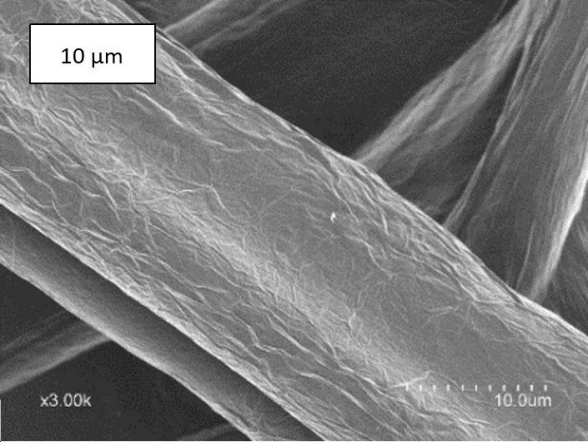
10 µm
x3.00k
10.0um

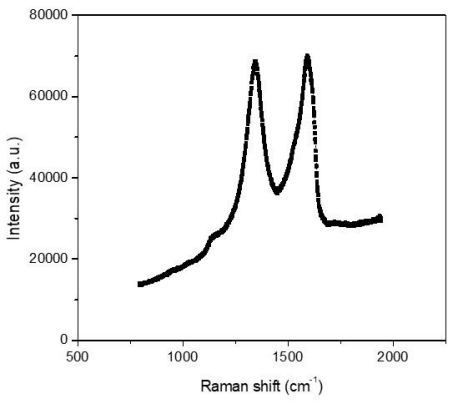
80000
60000
40000
20000
0
Intensity (a.u.)
500
1000
1500
2000
Raman shift (cm-1)

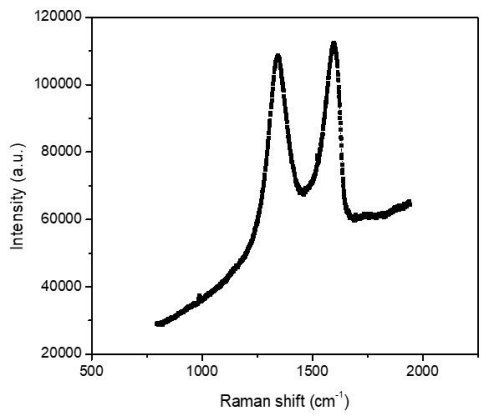
120000
100000
80000
60000
40000
20000
Intensity (a.u.)
500
1000
1500
2000
Raman shift (cm-1)

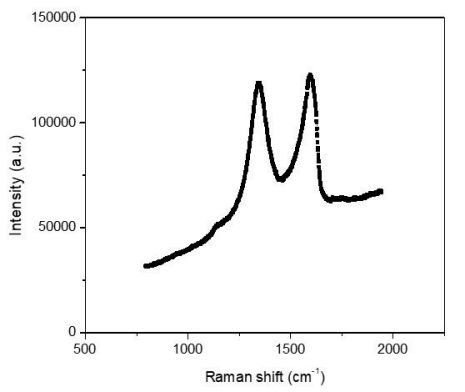
150000
100000
50000
0
Intensity (a.u.)
500
1000
1500
2000
Raman shift (cm-1)

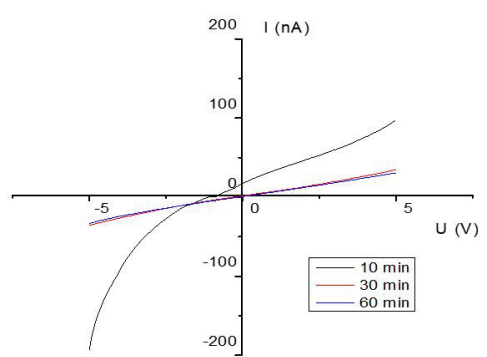

1 mg/mL

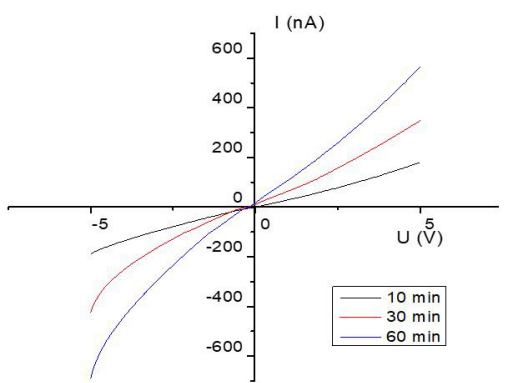

2 mg/mL

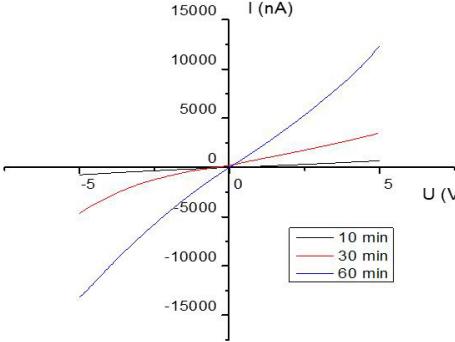
I (nA)
15000
10000
5000
0
-5000
-10000
-15000
-5
0
5
U (V)
10 min
30 min
60 min

4 mg/mL

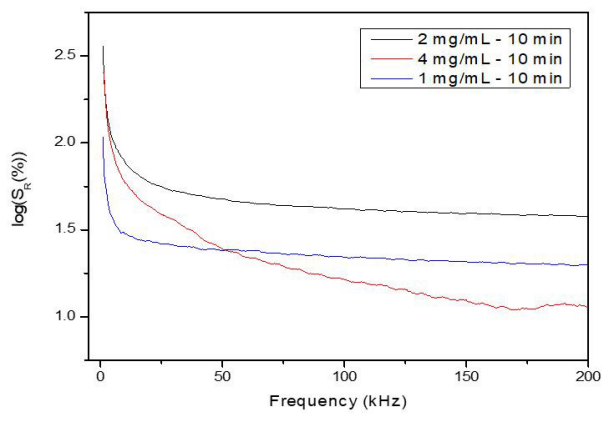
2 mg/mL - 10 min
4 mg/mL - 10 min
1 mg/mL - 10 min
log(S_R(%))
2.5
2.0
1.5
1.0
0
50
100
150
200
Frequency (kHz)

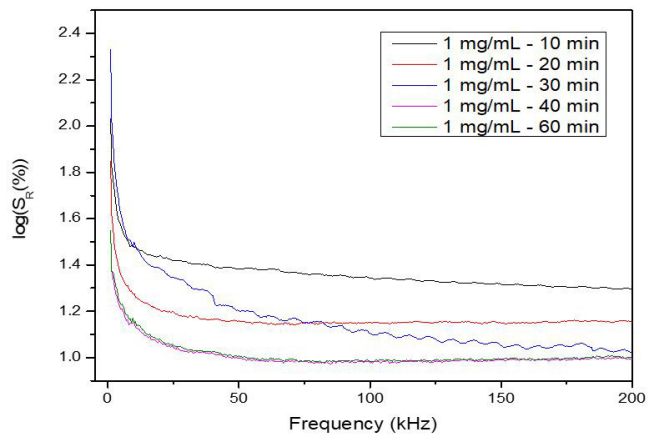
1 mg/mL - 10 min
1 mg/mL - 20 min
1 mg/mL - 30 min
1 mg/mL - 40 min
1 mg/mL - 60 min
log(S_R(%))
2.4
2.2
2.0
1.8
1.6
1.4
1.2
1.0
0
50
100
150
200
Frequency (kHz)

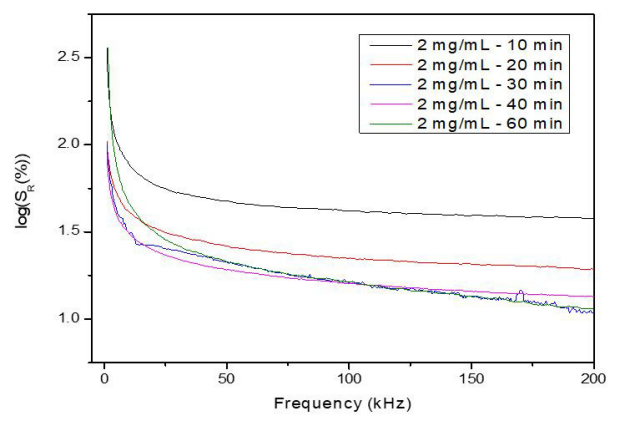
2 mg/mL - 10 min
2 mg/mL - 20 min
2 mg/mL - 30 min
2 mg/mL - 40 min
2 mg/mL - 60 min
log(S_R(%))
2.5
2.0
1.5
1.0
0
50
100
150
200
Frequency (kHz)

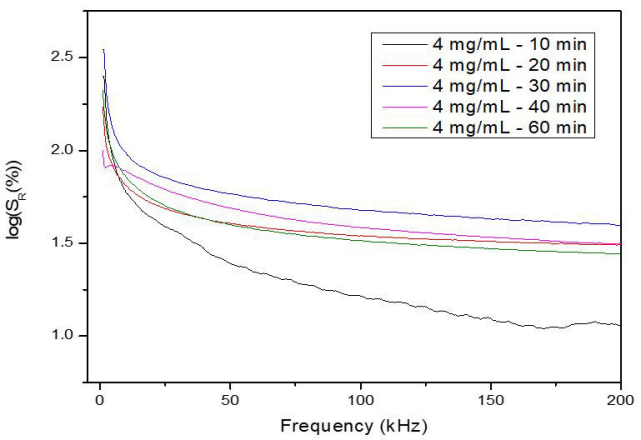
4 mg/mL - 10 min
4 mg/mL - 20 min
4 mg/mL - 30 min
4 mg/mL - 40 min
4 mg/mL - 60 min
log(S_R(%))
2.5
2.0
1.5
1.0
0
50
100
150
200
Frequency (kHz)

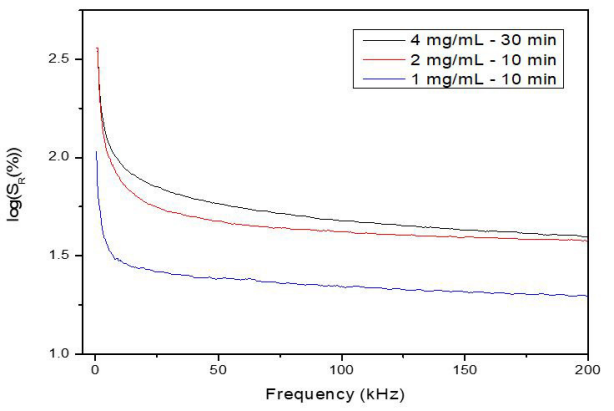
4 mg/mL - 30 min
2 mg/mL - 10 min
1 mg/mL - 10 min
log(S_R(%))
2.5
2.0
1.5
1.0
0
50
100
150
200
Frequency (kHz)

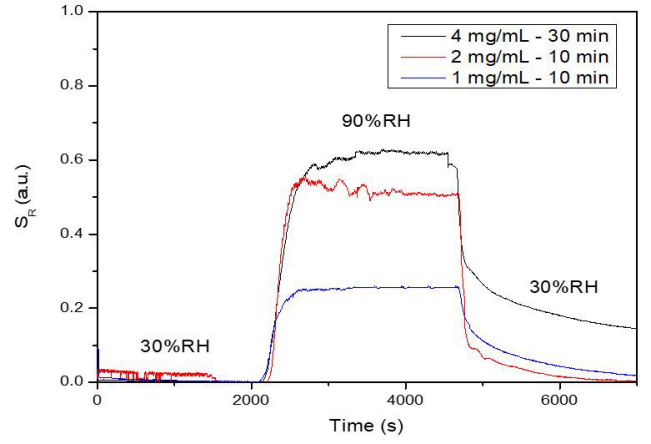
4 mg/mL - 30 min
2 mg/mL - 10 min
1 mg/mL - 10 min
90%RH
30%RH
30%RH
S_R (a.u.)
Time (s)
0.0
0.2
0.4
0.6
0.8
1.0
0
2000
4000
6000

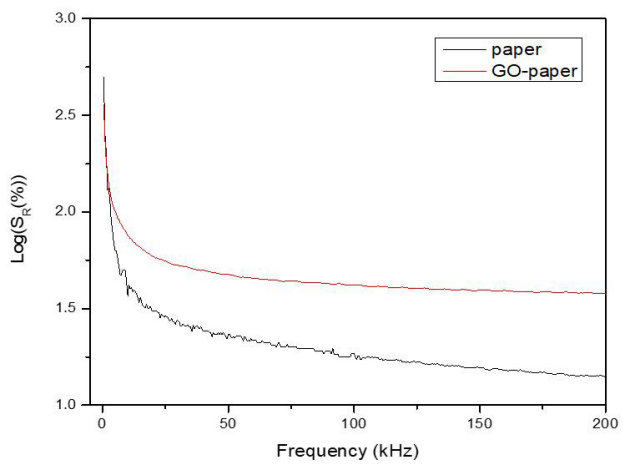
paper
GO-paper
3.0
2.5
2.0
1.5
1.0
Log(S_R(%))
0
50
100
150
200
Frequency (kHz)

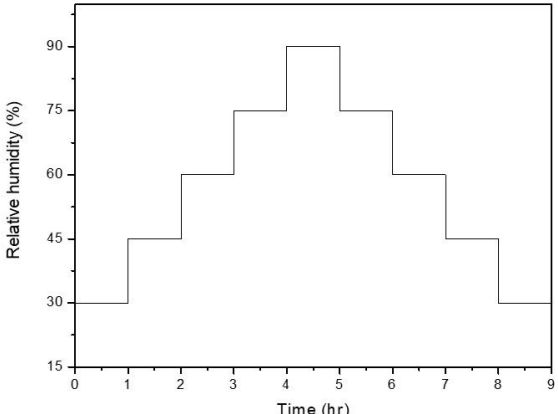
Relative humidity (%)
90
75
60
45
30
15
0
1
2
3
4
5
6
7
8
9
Time (hr)

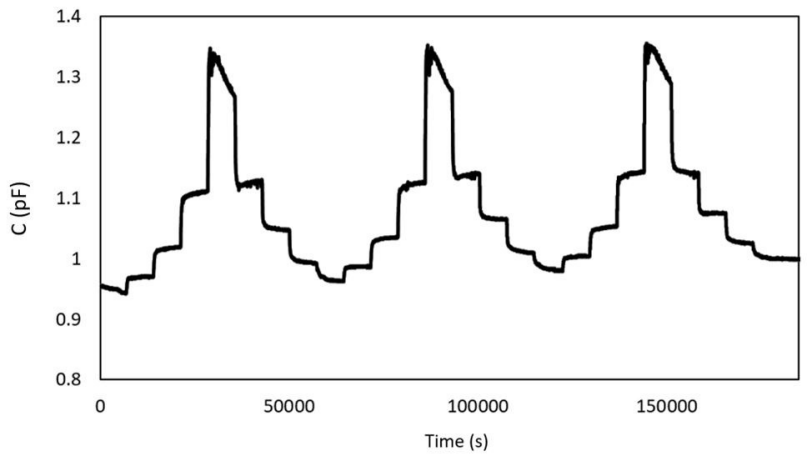
1.4
1.3
1.2
1.1
1
0.9
0.8
C (pF)
0
50000
100000
150000
Time (s)

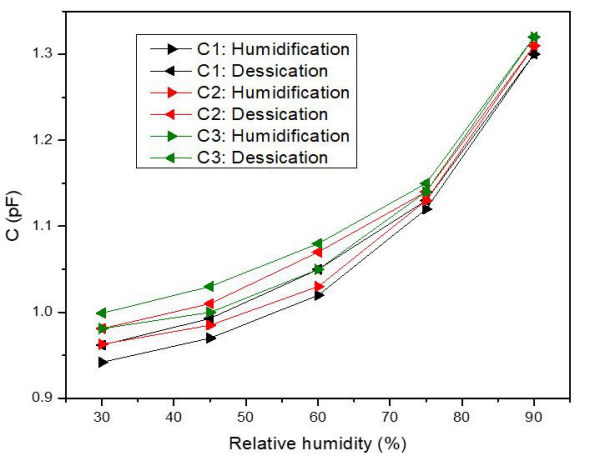
C1: Humidification
C1: Dessication
C2: Humidification
C2: Dessication
C3: Humidification
C3: Dessication
C (pF)
Relative humidity (%)
0.9
1.0
1.1
1.2
1.3
30
40
50
60
70
80
90

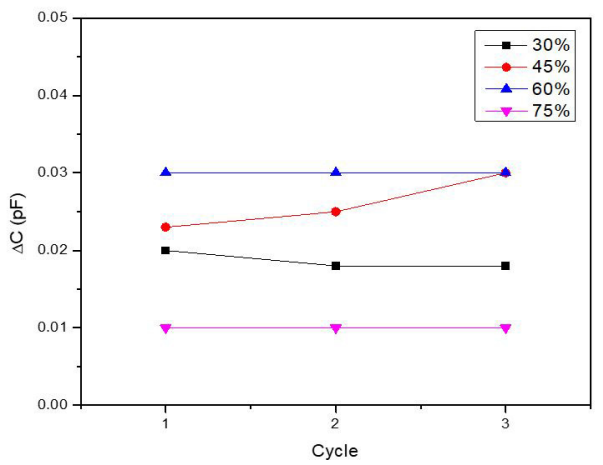
0.05
0.04
0.03
0.02
0.01
0.00
ΔC (pF)
1
2
3
Cycle
30%
45%
60%
75%

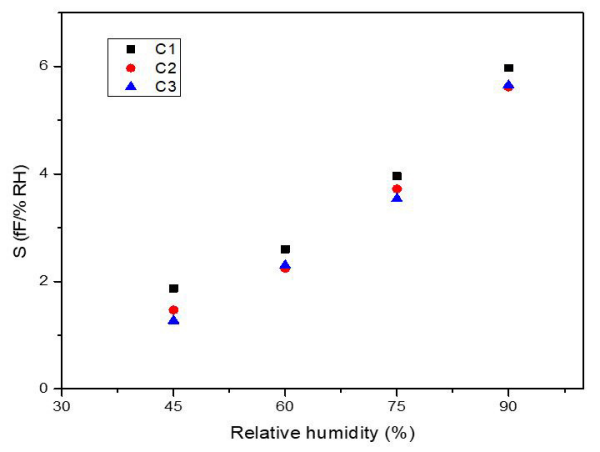
C1
C2
C3
S (fF/% RH)
0
2
4
6
30
45
60
75
90
Relative humidity (%)

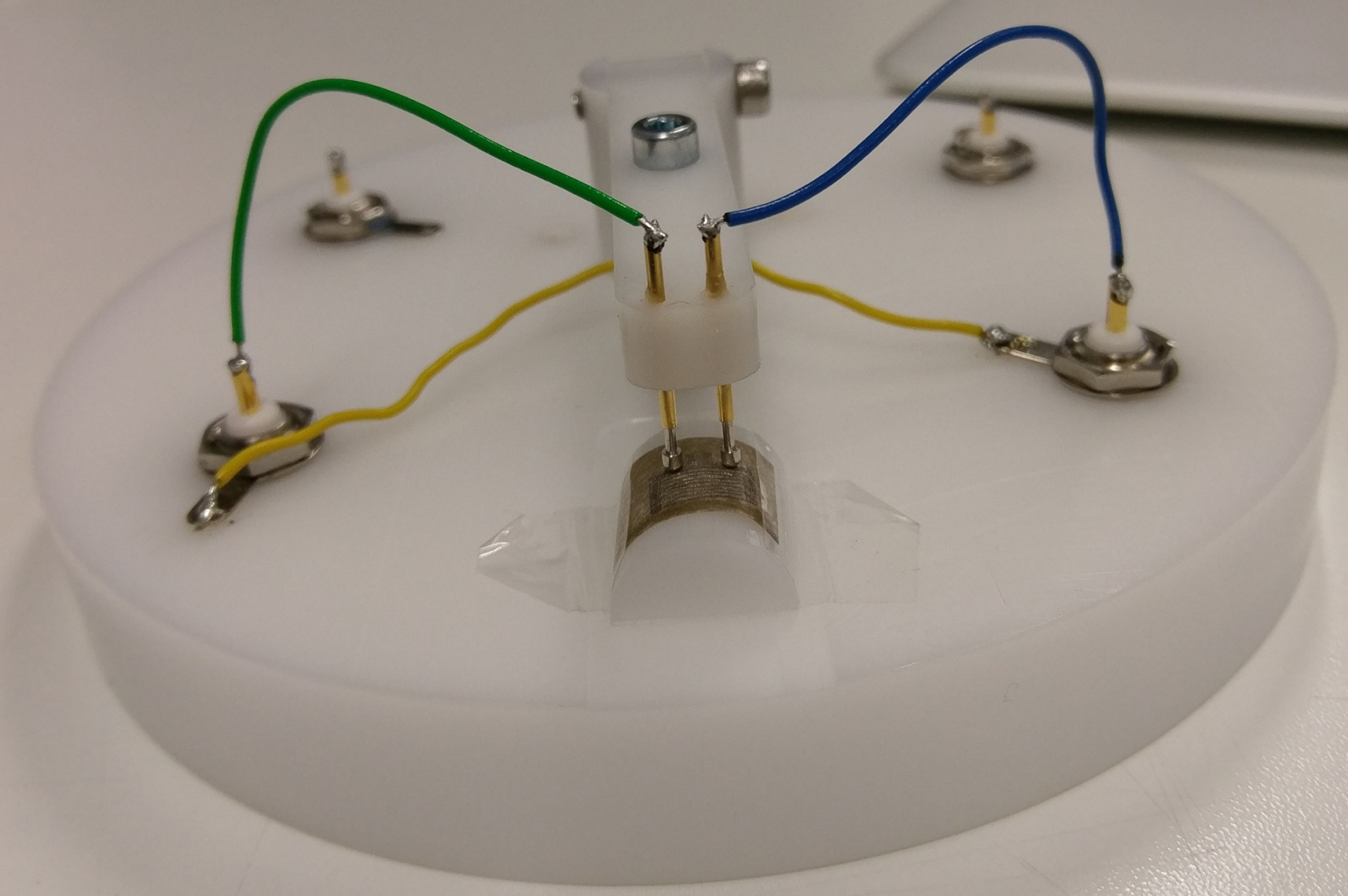

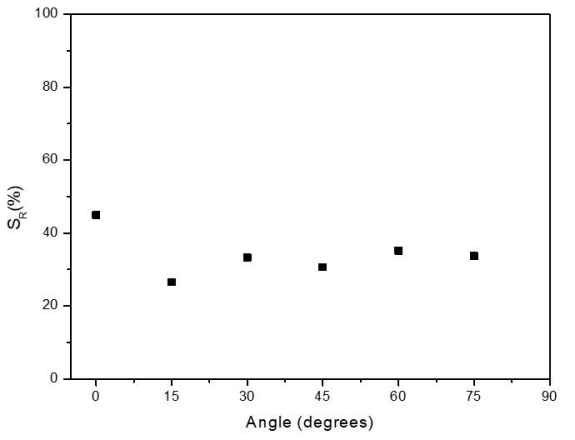
100
80
60
40
20
0
S_R(%)
0
15
30
45
60
75
90
Angle (degrees)

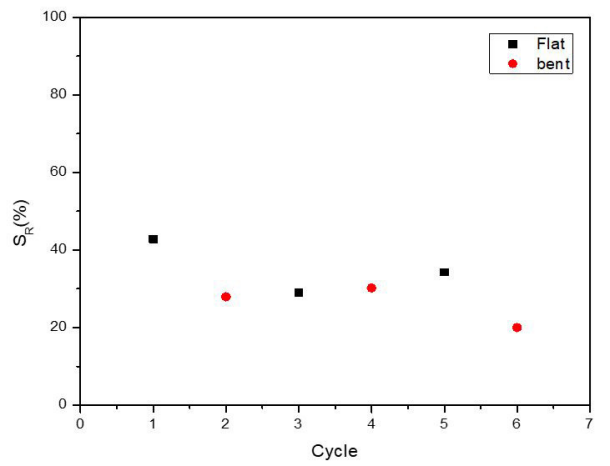
Flat
bent
S_R(%)
Cycle
0
20
40
60
80
100
0
1
2
3
4
5
6
7

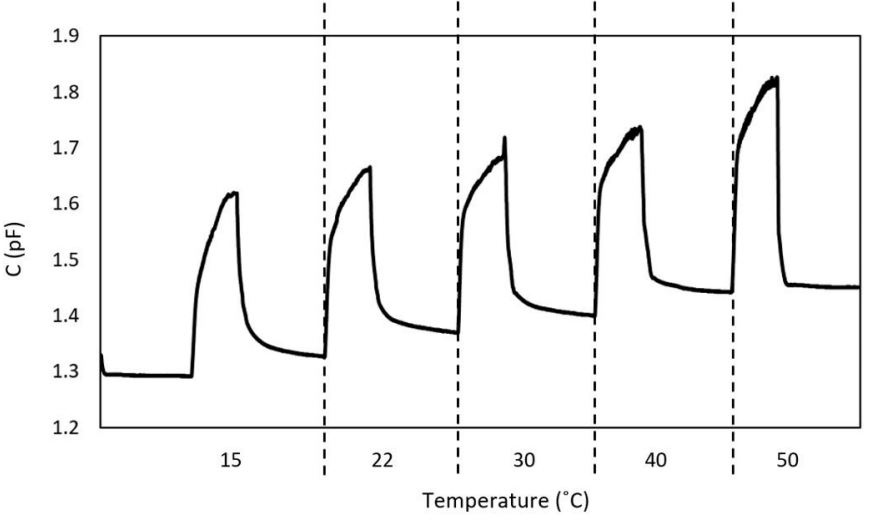
1.9
1.8
1.7
1.6
1.5
1.4
1.3
1.2
C (pF)
15
22
30
40
50
Temperature (˚C)

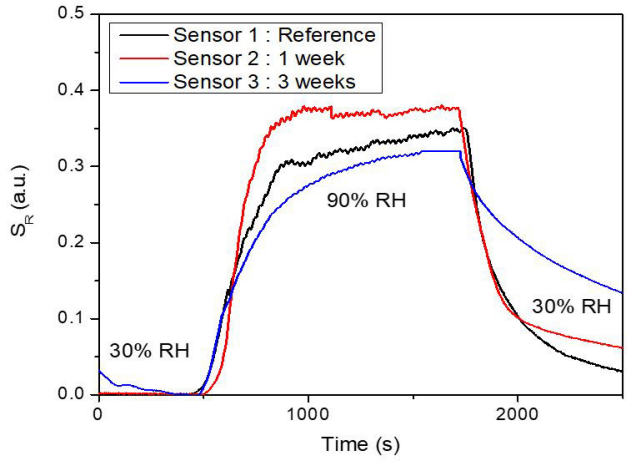
Sensor 1 : Reference
Sensor 2 : 1 week
Sensor 3 : 3 weeks
90% RH
30% RH
30% RH
S_R (a.u.)
Time (s)
0.0
0.1
0.2
0.3
0.4
0.5
0
1000
2000

Immersion time (min)	*1 mg/mL*	*2 mg/mL*	*4 mg/mL*
10	47.55	29.56	7.34
30	152.58	15.43	1.42
60	164.94	9.17	0.42

Exposure cycle	1	2	3
Relative response (%)	38	34.99	34.55
Sensitivity (fF/%RH)	5.97	5.62	5.65

Temperature (˚C)	15	20	30	40	50
Relative response (%)	25.23	25.39	24.84	24	26.4
Capacitance shift after desorption(%)	2.8	3	2.4	3.2	0.4

Target gas	Sensing material	Substrate	Fabrication technique	Sensitivity	Flexibility	Ref.
NO_2	CNT	Cellulosic paper	Inkjet printing	Cg[1]=10 ppm S[2]= 35% ($\Delta R/R_0$) RT[3]	R[4]=10 MΩ for 0˚≤θ[5]≤180˚ (inward) Not tested under NO_2	[41]
Cl_2	CNT	Cellulosic paper	Inkjet printing	Cg∼20 ppm S∼40% ($\Delta R/R_0$) RT	R=10 MΩ for 0˚≤θ≤180˚ (inward) Not tested under Cl_2	[41]
NH_3	CNT	Cellulosic paper	Drop-casting	Cg=50 ppm S=2% ($\Delta R/R_0$) RT	--	[40]
	CNT	Cellulosic paper	Papermaking filtration	Cg=50 ppm S=1% ($\Delta R/R_0$) RT	--	[40]
	MWCNTs	Paper	Plasma jet printing	Cg=60 ppm S=4% ($\Delta R/R_0$) RT	--	[42]
H_2O	CNT	Cellulosic filter paper	Drop-casting	Cg= [10,60]% RH S= 65% ($\Delta G/G_0$) RT	--	[19]
	rGO - PDDA	PI	Layer-by-layer nanoassembly	Cg= 52% RH S=20.91% ($\Delta R/R_0$) RT	--	[33]
	Graphene oxide - PDDA	PI	Layer-by-layer self-assembly	Cg=[11:97]% RH S=1552.3 pF/% RH F=10 kHz RT	--	[29]
	Graphene oxide - Gold Nps - Thiolated silica	PET	Sol-gel and self-assembly	Cg=[20:90]% RH S=0.0281 (logZ/% RH) F=1 kHz RT	Deviation = 13.6% θ=40˚ Cg=60% RH	[54]
	Graphene oxide - Diamine	PET	Brush-coating	Cg=[20:90]% RH S=0.0545 (logZ/% RH) F=1 kHz	Deviation = 4% θ=60˚ Cg=60% RH	[55]
	rGO – SnO_2	PI	Drop-casting	Cg=[11:97]% RH S=1604.89 pF/% RH ($\Delta C/\Delta RH$) F=10 kHz RT	--	[27]
	Graphene oxide nanoflowers – SnS_2	PET	Drop-casting	Cg=[11:97]% RH S=65 396 ($\Delta Z/\Delta RH$) F=100 Hz RT	--	[20]
	Graphene oxide – cellulose nanocrystals	PET	Drop-casting	Cg=[10:90]% RH S=54700% ($\Delta C/C_0$) F=1 kHz RT	--	[23]
	Graphene oxide - ZnO	PI	Layer-by-layer self-assembly	Cg=[0:97]% RH S=17785,6 pf/% RH ($\Delta C/\Delta RH$) F=100 Hz RT	--	[28]

Graphene oxide	**Paper**	**Self-assembly**	**Cg=[30,90]% RH** **S~209% ($\Delta C/C_0$)** **at 1 kHz** **S~38% ($\Delta C/C_0$)** **at 40 kHz** **RT**	**R= 11 MΩ for θ≤45˚** **R=26 MΩ for θ≥60˚** **S=30% for 15˚≤θ≤75˚** **(outward)** **Deviation = 12% for** **15˚≤θ≤75˚** **(outward)** **Cg=90% RH**	**This work**

[1]Cg : concentration of the target gas
[2]S : Sensitivity
[3]RT : Room temperature
[4]R: Resistance
[5]θ: Bending angle